J|A|C|S
ARTICLES

Morphology and Electronic Structure of the Oxide Shell on the Surface of Iron Nanoparticles

Chongmin Wang,*,† Donald R. Baer,† James E. Amonette,‡ Mark H. Engelhard,† Jiji Antony,§ and You Qiang§

Environmental Molecular Sciences Laboratory, and Fundamental and Computational Sciences Directorate, Pacific Northwest National Laboratory, P.O. Box 999, Richland, Washington 99352, and Physics Department, University of Idaho, Moscow, Idaho 83844-0903

Received January 16, 2009; E-mail: chongmin.wang@pnl.gov

Abstract: An iron (Fe) nanoparticle exposed to air at room temperature will be instantly covered by an oxide shell that is typically ~3 nm thick. The nature of this native oxide shell, in combination with the underlying Fe^0 core, determines the physical and chemical behavior of the core−shell nanoparticle. One of the challenges of characterizing core−shell nanoparticles is determining the structure of the oxide shell, that is, whether it is FeO, Fe_3O_4, γ-Fe_2O_3, α-Fe_2O_3, or something else. The results of prior characterization efforts, which have mostly used X-ray diffraction and spectroscopy, electron diffraction, and transmission electron microscopic imaging, have been framed in terms of one of the known Fe−oxide structures, although it is not necessarily true that the thin layer of Fe oxide is a known Fe oxide. In this Article, we probe the structure of the oxide shell on Fe nanoparticles using electron energy loss spectroscopy (EELS) at the oxygen (O) *K*-edge with a spatial resolution of several nanometers (i.e., less than that of an individual particle). We studied two types of representative particles: small particles that are fully oxidized (no Fe^0 core) and larger core−shell particles that possess an Fe core. We found that O *K*-edge spectra collected for the oxide shell in nanoparticles show distinct differences from those of known Fe oxides. Typically, the prepeak of the spectra collected on both the core−shell and the fully oxidized particles is weaker than that collected on standard Fe_3O_4. Given the fact that the origin of this prepeak corresponds to the transition of the O 1s electron to the unoccupied state of O 2p hybridized with Fe 3d, a weak pre-edge peak indicates a combination of the following four factors: a higher degree of occupancy of the Fe 3d orbital; a longer Fe−O bond length; a decreased covalency of the Fe−O bond; and a measure of cation vacancies. These results suggest that the coordination configuration in the oxide shell on Fe nanoparticles is defective as compared to that of their bulk counterparts. Implications of these defective structural characteristics on the properties of core−shell structured iron nanoparticles are discussed.

I. Introduction

Over the past few years, potential applications of Fe nanoparticles have been widely explored, including their use for drug delivery, enhanced magnetic resonant imaging (MRI),[1] information storage,[2] reduction of carbon dioxide,[3] and groundwater remediation.[4,5] Iron nanoparticles can be fabricated by a variety of methods, including Fe−oxide reduction in hydrogen at high temperature, sputter gas condensation,[6] and wet-chemical methods.[7−9] The morphology, particle size, and size distribution of the Fe nanoparticles show strong dependence on the synthesis process and processing parameters.[10] Regardless of the synthesis method or particle morphology, metal particles are oxidized when exposed to air or O.[11,12] At room temperature, this initial oxidation leads to a thin oxide shell that is typically ~2−3 nm thick.[13] Unless protected by some other type of layer, Fe^0 nanoparticles exposed to air will always be covered by a thin

† Environmental Molecular Sciences Laboratory, Pacific Northwest National Laboratory.
‡ Fundamental and Computational Sciences Directorate, Pacific Northwest National Laboratory.
§ Physics Department, University of Idaho.

(1) Qiang, Y.; Antony, J. J.; Sharma, A.; Nutting, J.; Sikes, D.; Meyer, D. *J. Nanopart. Res.* **2006**, *8*, 489–496.
(2) Zhang, X. X.; Wen, G. H.; Huang, S. M.; Dai, L. M.; Gao, R. P.; Wang, Z. L. *J. Magn. Magn. Mater.* **2001**, *231*, L9−L12.
(3) Tamaura, Y.; Tabata, M. *Nature* **1990**, *346*, 255–256.
(4) Nurmi, J. T.; Tratnyek, P. G.; Sarathy, V.; Baer, D. R.; Amonette, J. E.; Pecher, K.; Wang, C. M.; Linehan, J. C.; Matson, D. E.; Penn, R. L.; Driessen, M. D. *Environ. Sci. Technol.* **2005**, *39*, 1221–1230.
(5) Wang, C. B.; Zhang, W. X. *Environ. Sci. Technol.* **1997**, *31*, 2154–2156.
(6) Antony, J.; Qiang, Y.; Baer, D. R.; Wang, C. M. *J. Nanosci. Nanotechnol.* **2006**, *6*, 568–572.
(7) Peng, S.; Wang, C.; Xie, J.; Sun, S. *J. Am. Chem. Soc.* **2006**, *128*, 10676–10677.
(8) Cabot, A.; Puntes, V. F.; Shevchenko, E.; Yin, Y.; Balcells, L.; Marcus, M. A.; Hughes, S. M.; Alivisatos, A. P. *J. Am. Chem. Soc.* **2007**, *129*, 10358–10360.
(9) Peng, S.; Sun, S. H. *Angew. Chem., Int. Ed* **2007**, *46*, 4155–4158.
(10) Wang, C. M.; Baer, D. R.; Amonette, J. E.; Engelhard, M. H.; Antony, J.; Qiang, Y. *Nanotechnology* **2007**, *18*, 255603.
(11) Caberra, N.; Mott, N. F. *Rep. Prog. Phys.* **1948−1949**, *12*, 163–184.
(12) Fromm, E. *Kinetics of Matal-Gas Interactions at Low Temperature: Hydriding, Oxidation, Poisoning*; Springer: Berlin, Heidelberg, NY, 1998.
(13) Wang, C. M.; Baer, D. R.; Thomas, L. E.; Amonette, J. E.; Antony, J.; Qiang, Y.; Duscher, G. *J. Appl. Phys.* **2005**, *98*, 094308.

10.1021/ja900353f CCC: $40.75

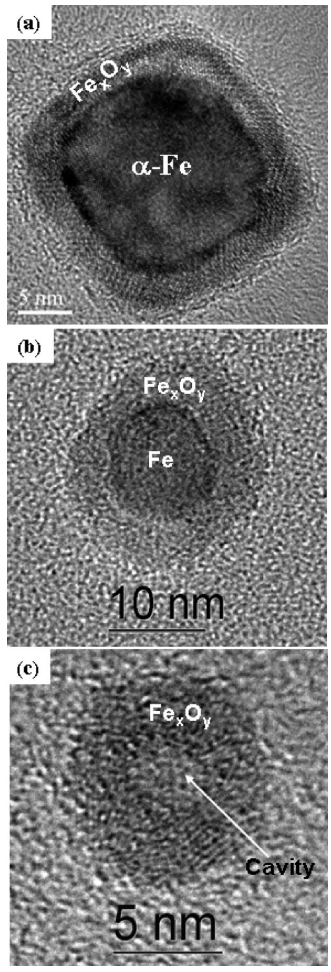

Figure 1. HRTEM images showing three types of Fe nanoparticles with core−shell structure: (a) faceted core−shell particle; (b) spherical core−shell particle; and (c) fully oxidized particle with a cavity at the center.

shell of oxide. The resulting particles are often described as core−shell Fe nanoparticles. Some properties of these core−shell nanoparticles depend on the size and shape of the metal particles and the nature of the oxide shell,[4] all of which can impact potential applications. For example, the biocompatibility of the Fe nanoparticles for medical applications may be controlled by the surface properties of the oxide shell.[1] Reduction of carbon tetrachloride by Fe has been observed to be influenced by the behavior of the surface oxide layers, which change with time in solution.[4,14]

Although the general microstructural features of the core−shell structured Fe nanoparticles have been well addressed as representatively shown in Figure 1,[10,13,15] the precise phase or structure of the oxide layers is not easily determined. Is the shell a single phase (consisting of wüstite (FeO), magnetite (Fe_3O_4), maghemite (γ-Fe_2O_3), hematite (α-Fe_2O_3), or an unknown phase), or is it a structure made up of layers of several phases? It is well established in high-temperature oxidation products, for example, that the phase and composition of the thick oxide layer formed on an Fe substrate depend on the distance of the layer from the innermost Fe-to-oxide interface such that a progression from Fe^0:FeO:Fe_3O_4:Fe_2O_3 occurs.[16] However, for the very thin oxide shell formed at room temperature on nanoparticles, it is hard to distinguish the spatial differences of the structure of the oxide shell as one moves from the external surface to the innermost Fe^0:oxide interface. On the basis of room temperature oxidation studies of single-crystal Fe(100) at ultrahigh vacuum (UHV),[17−26] it has been generally realized that the oxidation shell is composed of γ-Fe_2O_3/Fe_3O_4. In one instance, it was reported that FeO was formed initially and subsequent heating led to the transformation of FeO to γ-Fe_2O_3/Fe_3O_4.[21] Using in situ surface X-ray diffraction, Davenport et al.[27] and Toney et al.[28] found that the passive film formed on single-crystal Fe(110) and Fe(001) surfaces in a borate buffer solution was a new phase of Fe oxide: a spinel structure with a cation octahedral site occupancy of 80 ± 10%, a tetrahedral site occupancy of 66 ± 10%, and an octahedral interstitial site occupancy of 12 ± 4%. They observed that the passive film was composed of small nanocrystals that had an epitaxial orientation relationship with the Fe substrate. Mössbauer spectroscopy, X-ray photoelectron spectroscopy (XPS), and high-resolution transmission electron microscopy (HRTEM) have been used to probe the structural nature of the oxide shell on Fe nanoparticles.[29−38] The XPS and Mössbauer spectroscopy analyses have led to the notion that the oxide layer is dominated by γ-Fe_2O_3. On the basis of X-ray absorption spectroscopy analysis, Signorini et al. investigated the dependence of the phase of the oxide shell on the Fe nanoparticle size.[39] They

(14) Baer, D. R.; Tratnyek, P. G.; Qiang, Y.; Amonette, J. E.; Linehan, J. C.; Sarathy, V.; Nurmi, J. T.; Wang, C. M.; Antony, J. *Synthesis, Characterization and Properties of Zero Valent Iron Nanoparticles*; Imperial College Press: London, 2006.
(15) Wang, C. M.; Baer, D. R.; Amonette, J. E.; Engelhard, M. H.; Antony, M. J.; Qiang, Y. *Ultramicroscoy* **2007**, *108*, 43–51.
(16) Khanna, A. S. *Introduction to High Temperature Oxidation and Corrosion*; ASM International: Materials Park, OH, 2002.
(17) Leibbrandt, G. W.; Hoogers, G.; Habraken, F. H. P. M. *Phys. Rev. Lett.* **1992**, *68*, 1947.
(18) Brundle, C. R.; Chuang, T. J.; Wandelt, K. *Surf. Sci.* **1977**, *68*, 459–468.
(19) Brucker, C. F.; Rhodin, T. N. *Surf. Sci.* **1976**, *57*, 523–539.
(20) Roosendaal, S. J.; Asseelen, B. v.; Elsenaar, J. W.; Vredenberg, A. M.; Habraken, F. H. P. M. *Surf. Sci.* **1999**, *442*, 329–337.
(21) Simmons, G.; Dwyer, D. J. *Surf. Sci.* **1975**, *48*, 373–392.
(22) Ueda, K.; Shimizu, R. *Surf. Sci.* **1974**, *43*, 77–87.
(23) Leygraf, C.; Ekelund, S. *Surf. Sci.* **1973**, *40*, 609–635.
(24) Sewell, P. B.; Mitchell, D. F.; Cohen, C. *Surf. Sci.* **1972**, *33*, 535–552.
(25) Ruckman, M. W.; Chen, J.; Strongin, M. *Phys. Rev. B* **1992**, *45*, 14273–14278.
(26) Guo, T.; Boer, M. L. D. *Phys. Rev. B* **1988**, *38*, 3711–3717.
(27) Davenport, A. J.; Oblonsky, L. J.; Ryan, M. P.; Toney, M. F. *J. Electrochem. Soc.* **2000**, *147*, 2162–2173.
(28) Toney, M. F.; Davenport, A. J.; Oblonnsky, L. J.; Ryan, M. P.; Vitus, C. M. *Phys. Rev. Lett.* **1997**, *79*, 4282.
(29) Kwok, Y. S.; Zhang, X. X.; Qin, B.; Fung, K. K. *Appl. Phys. Lett.* **2000**, *77*, 3971–3973.
(30) Kuhn, L. T.; Bojesen, A.; Timmermann, L.; Nielsen, M. M.; Morup, S. *J. Phys.: Condens. Matter* **2002**, *14*, 13551–13567.
(31) Bianco, L. D.; Fiorani, D.; Testa, A. M.; Bonetti, E.; Savini, L.; Signoretti, S. *Phys. Rev. B* **2002**, *66*, 174418.
(32) Bodker, F.; Morup, S.; Linderoth, S. *Phys. Rev. Lett.* **1994**, *72*, 282–285.
(33) Gangopadhyay, S.; Hadjipanayis, G. C.; Dale, B.; Sorensen, C. M.; Klabunde, K. J.; Papaefthymiou, V.; Kostikas, A. *Phys. Rev. B* **1992**, *45*, 9778–9789.
(34) Haneda, K.; Morrish, A. H. *Nature* **1979**, *282*, 186–189.
(35) Rojas, T. C.; Lopez, J. C.; Greneche, J. M.; Conde, A.; Fernandez, A. *J. Mater. Sci.* **2004**, *39*, 4877–4885.
(36) Yi, W.; Moberly, W.; Chan, C.; Narayanamuri, V.; Hu, Y. F.; Li, Q.; Kaya, I.; Burns, M.; Chen, D. M. *J. Appl. Phys.* **2004**, *95*, 7136–7138.
(37) Shafranovsky, E. A.; Petrov, Y. I. *J. Nanopart. Res.* **2004**, *6*, 71–90.
(38) Moeck, P.; Fraundorf, P. *Z. Kristallogr.* **2007**, *222*, 634–645.
(39) Signorini, L.; Pasquini, L.; Savini, L.; Carboni, R.; Boscherini, F.; Bonetti, E.; Giglia, A.; Pedio, M.; Mahne, N.; Nannarone, S. *Phys. Rev. B* **2003**, *68*, 195423.

reported that the relative fraction of γ-Fe_2O_3 increased as the dimension of the Fe core decreased.

Thermodynamically, it has been generally expected that Fe−oxide nanoparticles are prone to either be disordered or transform to a different phase.[40] Such effects also occur in other systems. For example, with decreasing size, CeO_2 nanoparticles transform toward Ce_2O_3 (Ce^{3+}). Before a complete transformation, the cerium valence state shows spatial differences as one moves from the center to the surface of the particle.[41] These observations inspired us to raise similar questions about the nature of the thin oxide shell on Fe^0-core oxide-shell nanoparticles and the oxide "residue" remaining when small metal nanoparticles are fully oxidized.[13] The current understanding of the structure of the oxide shell on Fe nanoparticles is based on a combination of spectroscopic and diffractometric methods whose spatial resolution is larger than the key features of core−shell nanoparticles. Furthermore, the experimental results have been framed in terms of one of the known Fe−oxide structures, FeO, Fe_3O_4, γ-Fe_2O_3, or α-Fe_2O_3, despite the possibility that the structure of this thin oxide shell may deviate from the ideal structure of the known Fe oxides. In this Article, we report the results of direct probing of the structural nature of the oxide shell on individual Fe nanoparticles using EELS in a transmission electron microscope (TEM). This approach provides electronic structural information about the thin oxide shells on the Fe nanoparticles at a spatial resolution that is comparable to their size.

II. Experimental Section

The core−shell nanoparticles used for this work were synthesized using the cluster deposition method described in detail in previous papers[1,6] and summarized briefly here. Pure Fe particles were initially formed in a cluster source and deposited on a substrate. After deposition, they were exposed to ambient air, and the expected oxide layer formed on the surface of each nanoparticle. Monodispersive Fe nanoparticle sizes ranging from 2 to 100 nm can be formed depending on the helium-to-argon ratio, pressure inside the cluster source chamber, and the growth distance the clusters travel inside the cluster source chamber. The deposition rate was variable up to 10 mg/h, measured in situ with a rotatable quartz microbalance. The general structural features of the particles synthesized by this method have been reported in detail in previous publications.[10,13]

For TEM characterization, the nanoparticles were deposited on a carbon-film-coated copper grid. The data presented in this Article were obtained from the particles that have been on the TEM grid for about 3 years. The sample was kept in a drybox with flowing nitrogen. Taking into consideration the possible electron-beam damage, high spatial resolution, and energy resolution, EELS analysis was carried out using two microscopes at different laboratories. One microscope located at the Environmental Molecular Sciences Laboratory in Richland, WA, is a JEOL JEM-2010 TEM with a LaB_6 filament and postcolumn attached with a Gatan Image Filter (GIF2000). The acceleration voltage on the microscope is 200 kV. The EELS spectra were acquired in image-coupling mode (with a diffraction pattern on the TEM view screen). A 2 mm entrance aperture and an energy dispersion of 0.2 eV/channel were used. To improve the energy resolution, the LaB_6 filament was operated in an undersaturated condition. This configuration gave an energy resolution of 1.2 eV as measured by the full-width-at-half-magnitude of the zero-loss peak. Each spectrum acquisition time was typically ~10 s. The second microscope was a FEI Titan 80-to-300-kV Schottky field-emission microscope postcolumn attached with a GIF spectrometer (model Tridiem 863), located at FEI in Hillsboro, OR. The microscope was operated at 300 kV in the scanning transmission electron microscopy (STEM) mode with a probe size of ~2.0 Å. The GIF entrance aperture of 2 mm and an energy dispersion of 0.05 eV/channel were used, yielding an overall energy resolution of 0.9 eV. Initially, we expected the STEM EELS to enable high spatial resolution information. However, for the probe size of ~2 Å, the current and resulting intensity of the EELS spectrum were too low to yield useful information. To increase the signal intensity, the beam was scanned over the whole particle, and the EELS data acquisition time was 40 s. On the scale of a single nanoparticle, both microscopes gave consistent results. A power-law background was removed from the spectra. For data interpretation, we also collected both X-ray diffraction and EELS data on known bulk Fe_3O_4 powder particles, which were synthesized using a facile, solvent-free process described in detail elsewhere.[42] X-ray diffraction (XRD) patterns for nanoparticles mounted on a silicon wafer were collected with a Philips X'pert MPD diffractometer (model PW3040/00) using Cu Kα radiation, a 2θ scanning range of 10−80°, a step size of 0.05°, and a dwell time of 30 s at each step.

One factor to be considered during the electron-beam analysis is the possibility of electron-beam modification of the sample, including beam-induced oxidation and reduction. In a prior experiment, we observed that a core−shell nanoparticle with a metallic Fe core will be oxidized during electron beam irradiation in the TEM column with a typical vacuum of 10^{-5} Pa.[15] The oxidation process will normally lead to the growth of an oxide shell at a rate of 3 nm/h. This observation is in contrast to the typical result, that is, that an oxide will be reduced under the electron beam. Thus, it can be argued that the small fully oxidized particle will tend to be reduced during the electron beam analysis. However, we have not noticed any time-dependent effect on the EELS spectral features of our nanoparticles or of the standard Fe_3O_4 particles within a typical time for EELS acquisition of 180 s in total. Koyama et al. have studied the behavior of nickel oxide (NiO) under electron beam irradiation.[43] They noticed that the electron beam indeed led to reduction of the NiO to Ni^0, but within the time frame of several tens of minutes. For an electron-beam exposure of a few minutes, the reduction was not significant.

III. Results and Discussion

3.1. Structural Features Derived from X-ray and Electron Diffraction Analysis. The morphology and structural features of the core−shell Fe nanoparticles with respect to the particle size, shell thickness, and crystallographic orientation relationship between the Fe core and the oxide shell have been reported in previous publications.[10,13,15] In this Article, we concentrate on the atomic-level structure of the oxide shell as compared to a known ideal Fe oxide such as Fe_3O_4.

Two types of nanoparticles distinguished by their size were studied in detail in this work. One particle size is narrowly distributed around 7 nm. This type of particle is fully oxidized, and each particle contains a cavity at the center of the particle.[10,13] The low magnification TEM image of Figure 2a shows the general morphology of this type of particle. Figure 2b shows the XRD pattern of the particles. Because of the small particle size, the peaks in the XRD pattern are relatively broad. Based on the measured *d*-spacing, the XRD pattern suggests that this type of particle is composed of either Fe_3O_4 or γ-Fe_2O_3 or a mixture of both (distinction of Fe_3O_4 from γ-Fe_2O_3 by XRD

(40) Navrotsky, A.; Mazeina, L.; Majzlan, J. *Science* **2008**, *319*, 1635–1638.
(41) Wu, L.; Widemann, H. J.; Moodenbaugh, A. R.; Klie, R. F.; Zhu, Y.; Welch, D. O.; Suenaga, M. *Phys. Rev. B* **2004**, *69*, 125415.
(42) Ye, X. R.; Daraio, C.; Wang, C. M.; Talbot, J. B.; Jin, S. *J. Nanosci. Nanotechnol.* **2006**, *6*, 852–856.
(43) Koyama, Y.; Mizoguchi, T.; Ikeno, H.; Tanaka, I. *J. Phys. Chem. B* **2005**, *109*, 10749–10755.

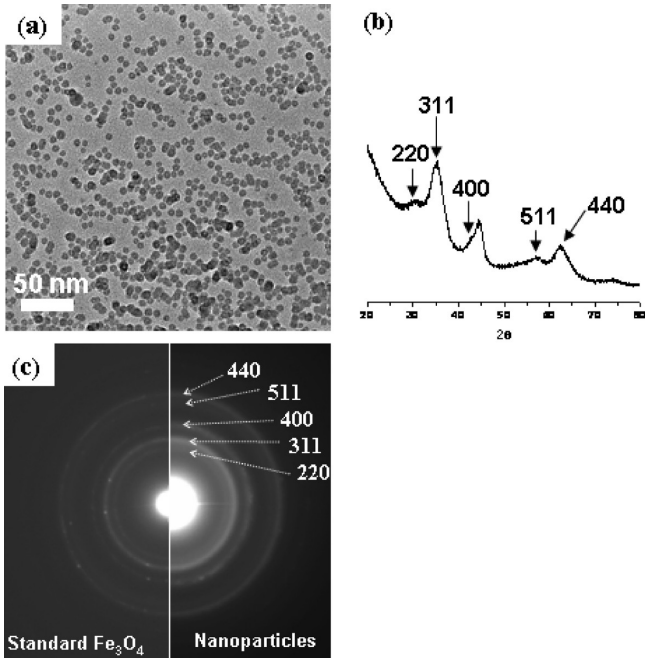

Figure 2. (a) TEM image of nanoparticles that have an average size of ~7 nm, most of which are fully oxidized to a hollow oxide; (b) XRD pattern collected on the particles shown in (a); and (c) comparison of the electron diffraction pattern obtained on the standard Fe_3O_4 specimen with that obtained on the particles shown in (a).

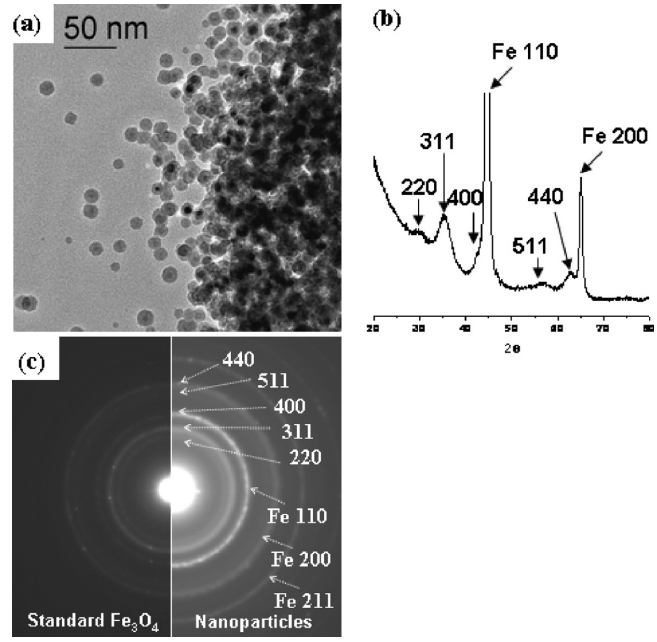

Figure 3. (a) TEM image of the nanoparticles with an average size of ~14 nm and the particles characterized as core−shell structured particles; (b) XRD pattern collected on the particles shown in (a); and (c) comparison of the electron diffraction pattern obtained on the standard Fe_3O_4 specimen with that obtained on the particles shown in (a).

is not possible for the nanoparticles). Figure 2c is a side-by-side comparison of the selected-area electron-diffraction patterns obtained on both a reference Fe_3O_4 (which is a well-characterized collection of Fe_3O_4 particles with diameters of 10−15 nm)[42] and our nanoparticles shown in Figure 2a. Although the electron diffraction pattern of the nanoparticle matches well with that of the reference Fe_3O_4, this does not necessarily indicate that the phase of the oxide shell is indeed Fe_3O_4. This is because, as was true for XRD, the electron diffraction ring patterns of Fe_3O_4 and γ-Fe_2O_3 are very similar. Both XRD and electron diffraction indicate that the oxide shell is either Fe_3O_4 or γ-Fe_2O_3 or a mixture of both. However, the data rule out the presence of an oxide shell consisting of FeO or α-Fe_2O_3.

The second type of particle has a diameter of ~14 nm, and each particle has an Fe core at the center of the particle as revealed by the TEM images shown in Figure 3a. Figure 3b shows the XRD pattern of this type of particle, which includes two strong metallic-Fe reflections, the (110) and (200). A comparison of the electron diffraction ring patterns of this nanoparticle with that of the reference Fe_3O_4 is shown in Figure 3b. As similarly concluded for the fully oxidized particles (Figure 2), both XRD and electron diffraction indicate that the oxide shell in this type of nanoparticle is either γ-Fe_2O_3 or Fe_3O_4 or a mixture of both, rather than FeO or α-Fe_2O_3. Differentiation of Fe_3O_4 from γ-Fe_2O_3 requires determination of the valence state of the Fe in the oxide and is discussed in the following section.

3.2. Electronic Structure Based on EELS Analysis. EELS spectra for a specific atomic species are influenced by both the coordination chemistry and the valence state of the atomic species being measured. For the Fe−oxide system, depending on the phase and the valence of Fe in the structure, three types of Fe−O coordination configurations are possible. The crystallographic data for FeO, Fe_3O_4, γ-Fe_2O_3, and α-Fe_2O_3 are summarized in Table 1. The structural features of these oxides, especially with respect to the coordination environment and valence state of Fe, are depicted in Figure 4.

FeO has the rock salt structure with space group *Fm*3*m* (225) and a lattice constant of 4.3088 Å.[44,45] The Fe has a valence of +2 and is ideally coordinated by six O atoms (octahedral configuration). However, the ideal FeO structure is rarely found in nature. The formula for the commonly observed structure can be described as FeO_{1-x}, which reflects two factors: (1) the presence of vacant cation sites and (2) the filling of some normally vacant tetrahedral sites by cations. These vacancies and occupied tetrahedral cation sites are not randomly distributed. The cation vacancies have been found to be distributed such that they form periodically spaced clusters, each cluster of neighboring octahedral cation sites being grouped around occupied tetrahedral cation sites.[45] The unit cell of the ideal FeO structure is shown in Figure 4a with the FeO_6 octahedral configuration.

Fe_3O_4 has the inverse spinel structure with space group *Fd*3*m* (227) and a lattice constant of 8.3941 Å.[46] In each unit cell, there are eight Fe_3O_4 formula units. The Fe in Fe_3O_4 has a mixed valence of Fe^{2+} and Fe^{3+} with a ratio of $Fe^{2+}/Fe^{3+} = 1/2$. The Fe occupies both tetrahedral and octahedral sites. There are a total of 64 tetrahedral sites and 32 octahedral sites in each unit cell, of which 8 of the 64 tetrahedral sites are occupied by the Fe^{3+} and 16 of the 32 octahedral sites are occupied by 8 Fe^{3+}

(44) Battle, P. D.; Cheetham, A. K. *J. Phys. C: Solid State Phys.* **1979**, *12*, 337–345.
(45) Koch, F.; Cohen, J. B. *Acta Crystallogr.* **1969**, *B25*, 275–287.
(46) Fleet, M. *Acta Crystallogr.* **1981**, *B37*, 917–920.
(47) Greaves, C. *J. Solid State Commun.* **1983**, *49*, 325–333.
(48) Shmakov, A. N.; Kryukova, G. N.; Tsybulya, S. V.; Chuvilin, A. L.; Solovyeva, L. P. *J. Appl. Crystallogr.* **1995**, *28*, 141–145.
(49) Olsen, J. S.; Cousins, C. S. G.; Gerward, L.; Jhans, H.; Sheldon, B. J. *Phys. Scr.* **1991**, *43*, 327–330.
(50) Perkins, D. A.; Attfield, J. P. *J. Chem. Soc., Chem. Commun.* **1991**, *202*, 229–231.

Table 1. Crystal Structure Data of Known Fe Oxides

	space group	lattice constant (Å)	atomic position	cation coordination environment	ref
FeO (Wüstite)	cubic *Fm*3*m* (225)	$a = 4.3088$	Fe^{2+}(4a) (0, 0, 0); O(4b) (0.5, 0.5, 0.5)	all Fe^{2+} occupy octahedral site	44, 45
Fe_3O_4 (Magnetite)	cubic (inverse spinel) *Fd*3*m* (227)	$a = 8.3941$	Fe^{3+}(8a) (0.125,0.125,0.125); Fe^{3+}/Fe^{2+}(16d) (0.5, 0.5, 0.5); O(32e) (0.2549,0.2549, 0.2549) (origin at center $-3m$, choice 2)	8 Fe^{3+} occupy 8 of total 64 tetrahedral sites, 8 Fe^{3+} and 8 Fe^{2+} randomly occupy 16 of the 32 octahedral sites	46
γ-Fe_2O_3 (Maghemite)	cubic $P4_332$ (212)	$a = 8.3474$	Fe^{3+} (0.9921, 0.9921, 0.9921); Fe^{3+}(0.865,0.615,0.875); Fe^{3+} (0.375,0.125,0.875) with 0.33 occupancy; O (0.861, 0.861, 0.861); O (0.372, 0.377, 0.876)	8 Fe^{3+} occupy tetrahedral sites, 13 1/3 Fe^{3+} and 2 2/3 cation vacancies occupy octahedral sites	48
α-Fe_2O_3 (Hematite)	rhombohedral $R\bar{3}c$ (167)	$a = 5.0352$, $c = 13.7508$	Fe^{3+}(c) (0, 0, 0.35517), O(e) 0.6950, 0, 0.25)	all Fe^{3+} occupy octahedral site	49, 50

and 8 Fe^{2+}. The unit cell of Fe_3O_4 is shown in Figure 4b with the Fe−O coordination environment.

γ-Fe_2O_3 possesses cubic symmetry with space group $P4_332$ (212) and a lattice constant of 8.3474 Å.[47,48] In ideal γ-Fe_2O_3, each unit cell includes 10 2/3 Fe_2O_3 formula units, which can be written as $(Fe_8)[Fe_{1\ 1/3}\square_{2\ 2/3}Fe_{12}]O_{32}$, where □ represents cation vacancy. Overall, Fe^{3+} occupies 8 of the total 64 tetrahedral sites, and 13 1/3 Fe^{3+} and 2 2/3 □ occupy 16 of the total 32 octahedral sites, leading to 3/8 of the Fe^{3+} ions in tetrahedral sites and 5/8 of the Fe^{3+} ions in octahedral sites. The □ (total 2 2/3 in each unit cell) are commonly observed to be ordered, thus resulting in the tetragonal superlattice structure of γ-Fe_2O_3 with a space group of $P4_12_12$ and a lattice constant of $a = 8.3474$ Å and $c = 25.0422$ Å.[47,48] The unit cell of the cubic structured γ-Fe_2O_3 is shown in Figure 4c with the Fe coordination depicted as well.

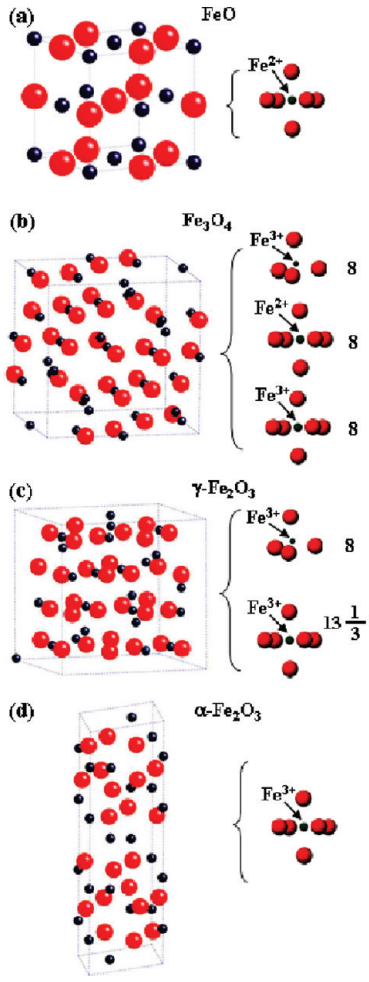

Figure 4. Crystallographic unit cell of different Fe oxides with the O−Fe coordinate unit illustrated at the right side: (a) FeO, (b) Fe_3O_4, (c) γ-Fe_2O_3, and (d) α-Fe_2O_3.

α-Fe_2O_3 has a corundum-type structure with the space group $R\bar{3}c$ (167) and lattice constants of $a = 5.03521$ Å and $c = 13.7508$ Å. Fe^{3+} occupies two-thirds of the octahedral sites confined by the nearly ideal hexagonal close-packed O lattice. A unit cell of α-Fe_2O_3 is shown in Figure 4d with the FeO_6 coordination environment.

The EELS fine structure of both the O *K*-edge and the Fe $L_{2,3}$-edges imprints these structural differences and therefore can be used to identify a specific Fe−oxide phase.[51−54] The valence state of Fe can often be determined from the following three aspects of the Fe $L_{2,3}$ EELS fine structure spectrum: chemical shift (dependence of the edge position with respect to the valence), fine structural features (splitting of the peaks), and the white-line ratios of the Fe L_2 and Fe L_3 spectra. Because of the uncertainty associated with the determination of the absolute energy loss scale, it is normally impossible to determine the valence state of Fe by the chemical shift method alone. EELS data obtained with an energy resolution of 0.5 eV will give fine structural features on the spectrum from which the valence state of Fe can be obtained. In this study, however, the spectral energy resolution of 0.9−1.2 eV did not allow us to extract the valence state of Fe using either of the first two methods. With respect to the third method, the Fe $L_{2,3}$ white line ratio, L_3/L_2, has been reported to be 3.3 for FeO, 3.4 for Fe_3O_4, and 3.6 for Fe_2O_3 by Sparrow et al.,[55] whereas Colliex et al.[51] reported that, depending on the peak-fitting methods, this ratio can range from 3.9 ± 0.3 to 4.6 ± 0.3 for FeO, from 4.2 ± 0.3 to 5.2 ± 0.3 for Fe_3O_4, from 4.4 ± 0.3 to 5.8 ± 0.3 for γ-Fe_2O_3, from 4.7 ± 0.3 to 6.5 ± 0.3 for α-Fe_2O_3. Because of this large variability and the peak-fitting method dependence of the white-line ratio, it is

(51) Colliex, C.; Manoubi, T.; Ortiz, C. *Phys. Rev. B* **1991**, *44*, 11402–11411.
(52) Paterson, J. H.; Krivanek, O. L. *Ultrmicroscopy* **1990**, *32*, 319–326.
(53) Wu, Z. Y.; Gota, S.; Jollet, F.; Pollak, M.; Gautier-Soyer, M.; Natoli, C. R. *Phys. Rev. B* **1997**, *55*, 2570–2577.
(54) Krishnan, K. M. *Ultramicroscopy* **1990**, *32*, 309–311.
(55) Sparrow, T. G.; Williams, B. G.; Rao, C. N.; Thomas, J. M. *Chem. Phys. Lett.* **1984**, *108*, 547.

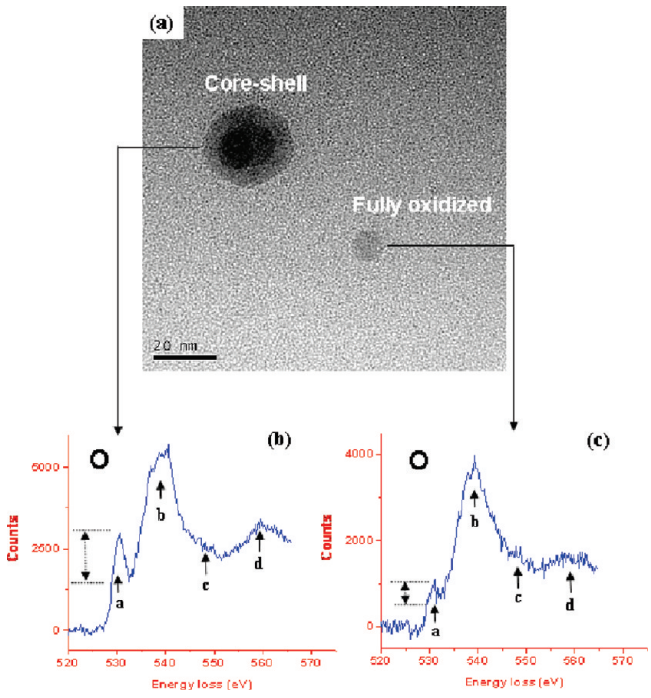

Figure 5. (a) TEM images of core−shell and fully oxidized particles. (b) O *K*-edge spectrum from the core−shell particle; and (c) O *K*-edge spectrum from the fully oxidized particle.

impossible to distinguish the phase of the oxide shell using the white-line ratio method alone. Furthermore, for the core−shell structured particles, the Fe $L_{2,3}$-edge contains contributions from both the zerovalent Fe in the core and the Fe within the oxide shell having an oxidation state of either +2 or +3. These complications minimize the value of using the Fe $L_{2,3}$-edge to distinguish phases in the core−shell particles. Fortunately, the O *K*-edge contains information solely contributed by the oxide shell, regardless of whether the particle has a core−shell structure or is fully oxidized. On the basis of these considerations, we concentrated on abstracting structural characteristics of the oxide shell from the fine features of the O *K*-edge.

Representative TEM images of the two particle types are shown in Figure 5a. The fully oxidized particle is relatively small and represents one of the particles shown in Figure 2a. The core−shell particle is relatively large, includes an Fe core, and represents one of the particles shown in Figure 3a. EELS spectra at the O *K*-edge collected on these two particles are shown in Figure 5b and c. The O *K*-edge spectra shown in Figure 5b and c are representative of several measurements made on particles of similar size and observed on the two different microscopes. These particles and the corresponding EELS spectra are shown as Supporting Information. Two significant features can be seen from Figure 5. First, the O *K*-edge collected on the particle that includes an Fe core (Figure 5b) is noticeably different from that collected on the fully oxidized particle (Figure 5c). Second, the O *K*-edge from the oxide shell shows distinct differences in the fine structure as compared to that obtained for oxides reported in the literature such as those reported for FeO, α-Fe_2O_3, γ-Fe_2O_3, and Fe_3O_4,[51,53] indicating that there are structural differences in the oxide shell as compared to the known Fe oxide structures. These two points are clearly illustrated by Figure 6, which is a side-by-side comparison of the EELS O *K*-edge obtained on both the core−shell structured nanoparticle and the fully oxidized nanoparticle with that obtained on the reference Fe_3O_4 nanocrystals. Colliex et al.[51] have systematically investigated the EELS O *K*-edge of FeO, Fe_3O_4, γ-Fe_2O_3, and α-Fe_2O_3 with an energy resolution of ∼1.0 eV, which is comparable to the ∼1.2 eV energy resolution used in our present work. Their EELS spectrum for Fe_3O_4 is nearly identical to our measurement for the reference Fe_3O_4. For example, the intensity ratio of prepeak *a* to main peak *b* for the Fe_3O_4 nanocrystals described here is measured to be ∼0.69 (measured from the peak height), which is close to the value of 0.68 we determine from the data presented by Colliex et al. for Fe_3O_4 powder particles.[51] The observations by Colliex et al. of the O *K*-edges on these well-defined oxides found features similar to what we observed for both the fully oxidized and the core−shell nanoparticles, but they differ in their relative peak heights. The EELS O *K*-edge spectral features shown in Figure 5 are related to the electronic states in the unoccupied conduction band of the nanoparticle. To understand the implications of the O *K*-edge fine structural features shown in Figure 5 on the possible structures of the oxide shell, we examined the origin of O *K*-edge fine structure features of known oxides and the correlation of each peak in the spectrum with the electronic structure of the oxide.

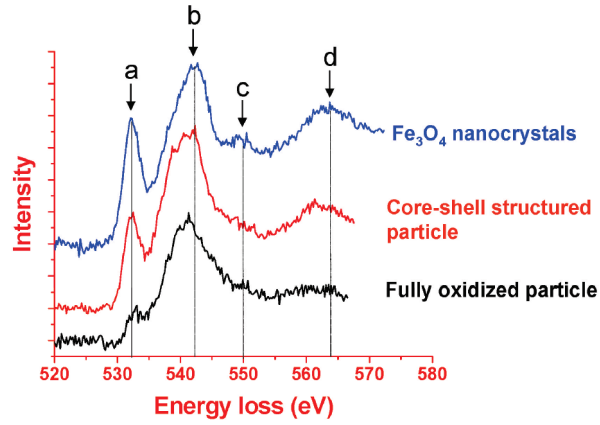

Figure 6. Comparison of the EELS O *K*-edge spectrum collected on the standard Fe_3O_4 nanocrystals, core−shell structured iron nanoparticle (as illustrated by the TEM image of Figure 1b), and small fully oxidized nanoparticles (no Fe core at the center of the particle as illustrated by the TEM of Figure 1c). To exclude the uncertainty for the absolute energy-loss scale, the prepeak was aligned at 532 eV, and, for clarity, each spectrum was vertically shifted.

3.2.1. Prepeak Features. The O *K*-edge shows four peaks, which are labeled *a*, *b*, *c*, and *d* in Figures 5 and 6. Qualitatively, the heights and the positions of these four peaks can be used to obtain information about the electronic structure and the coordination chemistry of the absorbing O atoms including information about (1) the valence state of Fe, (2) the average and distribution of the interatomic distances between the absorbing O and its nearest and next-nearest neighbors, (3) the nature of the Fe−O bond (degree of covalency vs ionicity), and (4) coordination number.

As is evident from Figure 6, significant differences can be seen in the intensity of the prepeak *a* for the standard Fe_3O_4, the core−shell structured nanoparticle, and the fully oxidized nanoparticle. The prepeak *a* is located at ∼532 eV, which can be interpreted as a transition from the O 1*s* core state to the unoccupied states of O 2p hybridized with the Fe 3d states. Therefore, the intensity of the prepeak *a* will reflect the unoccupied 3d state in the Fe atoms available for mixing with the O 2p states, as well as the bond length of Fe−O. This argument successfully explains the general observation that the intensity of the prepeak *a* relative to that of peak *b* increases in

the sequence FeO, Fe_3O_4, α-Fe_2O_3, and γ-Fe_2O_3.[51,53] Colliex et al. note that, relative to Fe_3O_4, α-Fe_2O_3, and γ-Fe_2O_3, FeO shows a very weak prepeak *a*.[51] They believe that this is because the Fe in FeO has a valence of +2 and a correspondingly longer Fe−O bond length (six Fe−O bonds at 2.15 Å) than the Fe in Fe_3O_4 (one Fe−O bond at 1.89 Å and three Fe−O bonds at 2.06 Å). Furthermore, it is known that the FeO is normally very defective with a large fraction of Fe vacancies.

We measured the ratio of prepeak *a* to peak *b* as 0.57 for the particle with an Fe core and 0.27 for the particle that is fully oxidized. Both of these values are significantly smaller than the value of 0.69 measured for the standard Fe_3O_4 nanocrystals. As discussed above, the height of prepeak *a* is related to the occupancy of the Fe 3d orbitals (and therefore the valence of Fe in the oxide), the coordination geometry around the absorbing O, and bond length between the absorbing O and the nearest neighbor Fe atoms. The weak prepeak *a* we observed on core−shell structured nanoparticles and fully oxidized nanoparticles therefore suggests the following structural differences between our nanoparticle specimens and the standard Fe_3O_4 specimen:

(1) The first is greater Fe^{2+} content in the oxide shell of the nanoparticle than in the standard Fe_3O_4. A high fraction of Fe^{2+} corresponds to a decrease of the hole population in the Fe 3d band that hybridizes with the O 2p state.[56] More broadly, this interpretation is also consistent with the general observation that across the transition-metal series the ratio of the prepeak to the main peak decreases with decreasing 3d hole on the metal site.[56,57] Therefore, this term appears to be the dominant factor for the observed weak prepeak of both the core−shell structured and the fully oxidized nanoparticles.

(2) The second is an increased Fe−O bond length in the oxide shell of the nanoparticles as compared to that in the standard Fe_3O_4. A longer Fe−O bond length will lead to a lesser degree of hybridization between the O 2p and Fe 3d orbitals. The bond length is also correlated with the valence state of the Fe.

(3) This third is a lower covalency of the Fe−O bond in the oxide shell of the nanoparticle than in the standard Fe_3O_4. In a pure Fe−O ionic bond model, the oxygen would have the configuration O $1s^2 2s^2 2p^6$ and the 1s→2p transition would be closed. Covalent bonding of Fe−O decreases the number of filled states with the O 2p character. Thus, the intensity of the prepeak is also related to the degree of covalency of the Fe−O bond. It is well-known that transition-metal oxides are not ionic and that the Fe−O bond has a considerable covalent nature.[56,58]

(4) The number of Fe atoms coordinated to each O is, on average, less than four for both the oxide shell of the core−shell structured nanoparticles and the fully oxidized nanoparticles. Decreasing the number of Fe atoms that coordinate to the O atom will decrease the available unoccupied density of states (available from empty Fe 3d bands), which will lead to a smaller prepeak.

A significant decrease is apparent in the intensity of the prepeak *a* for the relatively small and fully oxidized particle (Figures 5 and 6) relative to the core−shell structure particle and the standard Fe_3O_4. This result suggests that the above-discussed factors become more pronounced as the size of the nanoparticles decreases.

3.2.2. Features of peaks *b*, *c*, and *d*. The points discussed above based on the features of the prepeak *a* are also consistently supported by the subtle differences in peaks *b*, *c*, and *d* as shown in Figure 6. Colliex et al.[51] observed that peak *b* remains rather similar for FeO, Fe_3O_4, γ-Fe_2O_3, and α-Fe_2O_3. They note that peak *c* is a very weak peak, which shows dependence on the oxide phase but appears to be similar for Fe_3O_4 and γ-Fe_2O_3. Peak *d* is a rather broad peak that shows little distinction with respect to the known four different kinds of iron oxide. To exclude the uncertainty regarding the absolute energy scale, the spectra shown in Figure 6 are all aligned with the prepeak *a* at 532 eV. It is apparent that, as compared to the standard Fe_3O_4, peaks *b* and *d* from the oxide shell of both core−shell structured and the fully oxidized nanoparticles shift to lower energies, and such a shift appears to be pronounced with the fully oxidized particles. From the electronic transition point of view, peaks *b*, *c*, and *d* are generally attributed to the transition of the O 1s electron to O 2p unoccupied states hybridized with Fe unoccupied 4s and 4p states.[51,56] Shifting of both peaks *b* and *d* to lower energies suggests a high fraction of Fe^{2+} and increased O−Fe bond length in the oxide shell of nanoparticles as compared to that of the standard Fe_3O_4. These two points support the qualitative analysis based on the feature of prepeak *a* as described in section 3.2.1. Using a density function theory (DFT) calculation, Yoshiya et al.[59] have systematically calculated the EELS of both TiO_2 rutile and the rock-salt structured TiO_x ($x < 2$). They noticed that with the decrease of the *x* values, the separation between the main peak and the prepeak on the O *K*-edge decreases. The conclusions derived by Yoshiya et al. are supported by the EELS experimental results carried out by Mitterbauer et al.[60] and Weng et al.[61] for the system of TiO_x. On this basis, similar to the case of reduced TiO_x ($x < 2$), the presently observed shifting of peaks *b* and *d* toward prepeak *a* for the iron oxide system would be expected to indicate a high fraction of the Fe^{2+} in the oxide shell of both the core−shell structured and the fully oxidized nanoparticles as compared to the standard Fe_3O_4. From the point of view of scattering resonance, it is known that the position of the resonance energy, *E*, and the radius of the scattering shell, *R*, satisfies the relationship: $E^*R^2 = \text{constant}$.[53,62,63] Therefore, the resonance energy position scales inversely with the square of the radius of the scattering shell, thereby setting the basis for the increased Fe−O bond length.

It is evident from Figure 6 that, as compared to Fe_3O_4, peaks *c* and *d* of the O *K*-edge collected on both the core−shell structured and the fully oxidized particles are smeared out. Using a full multiple scattering approach, Wu et al.[53] have found that the major contributions to peak *c* are from single-scattering events between the O absorber and the 24 next-nearest neighbor O atoms. For Fe_3O_4, there are six O atoms at 5.07 Å, six atoms at 5.21 Å, and 12 atoms at 5.14 Å, giving an average distance of 5.14 Å between the absorbing O and this shell of O. Peak *d* derives dominantly from single-scattering events between the absorbing O atom and 12 nearest-neighbor O atoms for Fe_3O_4

(56) Groot, F. M. F.; Grioni, M.; Fuggle, J. C.; Ghijsen, J.; Sawatzky, G. A.; Petersen, H. *Phys. Rev. B* **1989**, *40*, 5715–5723.
(57) Kurita, H.; Lefevre, E.; Colliex, C.; Brydson, R. *Phys. Rev. B* **1993**, *47*, 13763.
(58) Tsukada, T.; Adachi, H.; Satoko, C. *Prog. Surf. Sci.* **1983**, *14*, 113–119.
(59) Yoshiya, M.; Tanaka, I.; Kaneko, K.; Adachi, H. *J. Phys.: Condens. Matter.* **1999**, *11*, 3217–3228.
(60) Mitterbauer, C.; Kothleitner, G.; Hofer, F. *Microsc. Microanal.* **2003**, *9*, 834–835.
(61) Weng, X.; Fisher, P.; Skowronski, M.; Salvador, P. A.; Maksimov, O. *J. Cryst. Growth* **2008**, *310*, 545–550.
(62) Ashley, C. A.; Doniach, S. *Phys. Rev. B* **1975**, *11*, 1279.
(63) Kutzler, F. W.; Ellis, D. E. *Phys. Rev. B* **1984**, *29*, 6890–6900.

(3 atoms at 2.85 Å, 6 atoms at 2.97 Å, and 3 atoms at 3.08 Å). An average distance of 2.97 Å between the absorbing O and this shell of O atoms is obtained. Given the origin of these peaks, smearing out of both peaks *c* and *d* indicates that the distribution of the interatomic distances between the absorbing O and the nearest as well as the next-nearest neighbor O atoms in the oxide shell is wider than that in the standard Fe_3O_4. This point could also be consistent with a relatively longer Fe−O bond length as discussed on the basis of the intensity feature of prepeak *a* and relative shifting of peaks *b* and *d* to lower energies. Furthermore, it has been established that the smaller and fully oxide nanoparticle is composed of small crystallites, which are separated by grain boundaries.[13] It is known that the atomic coordination environment in a grain boundary is normally distorted and compositionally deviates from the stoichiometry as compared to that in the bulk.[64,65] Therefore, grain boundaries in the smaller and fully oxidized particles also likely contribute to the observed obvious smearing out of the peaks *c* and *d*.

3.3. General Description of the Fine Structural Features. The above qualitative analysis of the EELS O *K*-edge fine structure feature leads to a pictorial description of the structural features for both the core−shell structured and the fully oxidized nanoparticles. As compared to Fe_3O_4, a higher fraction of Fe in the oxide shell exists as Fe^{2+} and has, correspondingly, a longer Fe−O bond length. This structural feature appears to be more pronounced for the fully oxidized particle. However, both XRD and electron diffraction indicate that the oxide shell cladding the surface of the Fe nanoparticle and the fully oxidized nanoparticles remains structurally as Fe_3O_4/γ-Fe_2O_3, rather than FeO. This result indicates that, as compared to the standard Fe_3O_4 particle, the oxide shell in the core−shell structured Fe nanoparticle is a defective structure. Although we have not carried out a systematic experiment regarding the dependence of the O *K*-edge feature on the particle size, the present observations and analysis of two types of representative particles clearly demonstrate that the oxide shells for the core−shell structured and fully oxidized particles are indeed different. Typically, the small and fully oxidized particle is even more defective than the particle with an Fe core. This point is consistent with the observation that the oxide shell cladding on a relatively large and well-faceted Fe atom is a single crystal and possesses a definitive crystallographic orientation with respect to the underlying Fe core. For the small and fully oxidized particle, the oxide shell normally exhibits a multidomain structure as reported in detail in prior publications.[10,13,15]

The present observation of the defective structural nature of the oxide shell seems to be consistent with the observations of Davenport et al.[27] and Toney et al.[28] They noticed that the passive film formed on single-crystal Fe(110) and Fe(001) surfaces in a borate buffer solution was a new phase of Fe oxide: a spinel structure with a cation octahedral site occupancy of 80 ± 10%, a tetrahedral site occupancy of 66 ± 10%, and an octahedral interstitial site occupancy of 12 ± 4%. Furthermore, the present observation appears to be consistent with the observation of Signorini et al. based on an X-ray absorption near-edge structure (XANES) study of a core−shell structured Fe nanoparticle with the Fe core in the size range of 7−21 nm.[39] They reported that the phase of the oxide shell depended on the particle size and that as the particle size decreases, the oxide shell assumes a γ-Fe_2O_3 structure. They further speculated that the local structure of the oxide shell on the Fe nanoparticle varies as a function of distance from the underlying Fe core. Thus, the outer surface of the oxide shell is expected to be γ-Fe_2O_3 and the inner region that is adjacent to the Fe core is expected to be Fe_3O_4. We note, however, that such a phase transition in the oxide shell has not been observed in a single particle. We expect that this could be experimentally resolved with high spatial resolution using a electron probe having an energy resolution of 0.5 eV where both the O *K*-edge and the Fe $L_{2,3}$-edge will show the finer structural features specific to different Fe oxides.

The structure and electronic structural features that we observed for core−shell and fully oxidized Fe nanoparticles, such as the relatively high fraction of Fe^{2+} and increased Fe−O bond length, are similar to that observed by Wu et al. for cerium oxide nanoparticles.[41] They noticed that the fraction of Ce^{3+} ions in the particles rapidly increased with decreasing particle size when the particle is below ∼15 nm in diameter. The particles were completely reduced to $CeO_{1.5}$ at the diameter of ∼3 nm. The reduced CeO_2 nanoparticle has a fluorite structure, which is the same as that of bulk CeO_2. They also noticed that for larger particles the valence reduction of cerium ions occurs mainly at the surface, forming a $CeO_{1.5}$ layer and leaving the core as essentially CeO_2. Furthermore, Wu et al.,[41] Tsuenekawa et al.,[66] and Zhang et al.[67] have noticed that the lattice constant of CeO_{2-x} increases with decreasing particle size. Although of different structures, both the Fe^0-core oxide-shell and the cerium oxide nanoparticles demonstrate the importance of particle size on metal−oxide bond length and the tendency of these nanoparticles to become increasingly defective as size decreases.

It is known that the behavior and properties of nanoparticles depend on their process method, handling history, and the environment in which the nanoparticles exist.[68] For example, the amount of $CeO_{1.5}$ in CeO_{2-x} nanoparticles is a strong function of the particular synthesis methods used to make these particles.[41,66,67] Therefore, it is likely that the structure and electronic structures we observed for the core−shell structured Fe nanoparticles and the fully oxidized nanoparticles are specific to these types of nanoparticles prepared by the present method. Fe nanoparticles prepared by other processes and having different handling histories may exhibit different structures.

3.4. Implication for the Properties of the Core−Shell Structured Fe Nanoparticles. The present study indicates that oxide shells of Fe nanoparticles are more defective than the bulk structures of Fe oxides. The defective structural nature of the oxide shells will influence their chemical, magnetic, and electronic properties. The defective structure would be expected to create reactive sites and mass-transport pathways that will alter the chemical reactivity of the nanoparticles as has been observed..[4,69−72] We have already observed, for example, that core−shell structured Fe nanoparticles prepared in different

(64) Sutton, A. P.; Balluffi, R. W. *Interfaces in Crystalline Materials*; Oxford University Press: Oxford, NY, 2006.
(65) Wynblatt, P.; Rohrer, G. S.; Papillon, F. *J. Eur. Ceram. Soc.* **2003**, *23*, 2841–2848.
(66) Tsunekawa, S.; Sivamohan, R.; Ito, S.; Kasuya, A.; Fukuda, T. *Nanostruct. Mater.* **1999**, *11*, 141–147.
(67) Zhang, F.; Chan, S. W.; Spanier, J. E.; Apak, E.; Jin, Q.; Robinson, R. D.; Herman, I. R. *Appl. Phys. Lett.* **2002**, 80.
(68) Baer, D. R.; Amonette, J. E.; Engelhard, M. H.; Gaspar, D. J.; Karakoti, A. S.; Kuchibhatla, S.; Nachimuthu, P.; Nurmi, J. T.; Qiang, Y.; Sarathy, V.; Seal, S.; Sharma, A.; Tratnyeke, P. G.; Wang, C. M. *Surf. Interface Anal.* **2008**, *40*, 529–537.
(69) Sarathy, V.; Tratnyek, P. G.; Nurmi, J. T.; Baer, D. R.; Amonette, J. E.; Wang, C. M.; Chun, C. L.; Lee Penn, N.; Lai, G.; Reardon, E. J. *J. Phys. Chem. C* **2008**, *112*, 2286–2293.
(70) Li, X. Q.; Elliott, D. W.; Zhang, W. X. *Crit. Rev. Solid State Mater. Sci.* **2006**, *31*, 111–222.

ways react with different rates and have different branching ratios when reducing carbon tetrachloride.[4,68] We have also observed that the introduction of additional Fe^{2+} into the shell oxide speeds the reaction rate and alters the branching ratio.[69]

The oxide shell also been observed to influence the magnetic properties of the types of core−shell particles we have examined. The use of high magnetic moment core−shell nanoparticles for biomedical applications dramatically enhanced the contrast for MRI, reduced the concentration of magnetic particle needs for cell separation, or made drug delivery possible with much lower magnetic field gradients. Fe core−shell nanoparticles prepared by the current method exhibit an increased coercivity and exchange bias relative to Fe_3O_4, and the exchange bias increases with the thickness of the oxide shell.[73] For ideally structured Fe_3O_4, the spin moments of all of the Fe^{3+} ions on the octahedral sites are aligned parallel to one another, but directed oppositely to the spin moments of the Fe^{3+} ions occupying the tetrahedral positions. Therefore, the magnetic moments of all Fe^{3+} ions theoretically cancel each other and make no contribution to the magnetization of the solid. However, the magnetic moments of all of the Fe^{2+} ions are aligned parallel to one another and are responsible for the net magnetization of the solid.[74] Because of the difference in magnetic moments of the two valence states of Fe (5.92 μ_B for Fe^{3+} and 4.90 μ_B for Fe^{2+}, where μ_B is the Bohr magneton), a change in the fraction of Fe^{2+} ions in the oxide shell of the nanoparticles relative to the ideal Fe_3O_4 structure will have a significant impact on the magnetic properties of the whole particle. The specific magnetic moment of core−shell Fe nanoparticles is size dependent and increases rapidly from about 80 emu/g at the size of around 3 nm to over 210 emu/g up to the size of 100 nm (about 10 times higher than the commercial Fe oxide nanoparticle).[1]

IV. Conclusions

The structural features of the oxide shells found on Fe nanoparticles were studied using a combination of XRD, electron diffraction, and EELS on the O *K*-edge. The O *K*-edge shows fine structural features that are similar to those exhibited by Fe_3O_4, but with differences in peak intensities and position. The pre-edge peak obtained on both the core−shell structured nanoparticles and the fully oxidized nanoparticles is weaker than that of Fe_3O_4. On the basis of what is known about the origin of this pre-edge peak structure, we conclude that the oxide shell in the core−shell structured Fe nanoparticle is highly defective in comparison to the equivalent oxide of bulk form. Qualitatively, the observed spectra correspond to a higher degree of occupancy of the Fe 3d orbital, a longer Fe−O bond length, a decreased covalency of the Fe−O bond, and a larger number of Fe ion vacancies relative to magnetite crystals. The defective structure of the oxide shell is expected to influence the chemical activity, lifetime in aqueous solution, and magnetic properties of the nanoparticles. We have demonstrated that EELS is a powerful tool to probe fine structural features of nanoparticles with a high spatial resolution, thereby complementing X-ray absorption spectroscopy studies. In future work, we plan to examine the changes in oxide electronic structure as a function of particle size as well as particle surface structure.

Acknowledgment. We appreciate the effort of Dr. Y. C. Wang from FEI in Hillsboro, OR, in acquiring the EELS spectra using the Titan microscope. This work was supported by the U.S. Department of Energy (DOE) Office of Science, Offices of Basic Energy Sciences and Biological and Environmental Research. Part of the work was conducted at the William R. Wiley Environmental Molecular Sciences Laboratory (EMSL), a national scientific user facility sponsored by DOE's Office of Biological and Environmental Research and located at Pacific Northwest National Laboratory (PNNL). PNNL is operated by Battelle for the DOE under contract DE-AC06-76RLO 1830. The work carried out at the University of Idaho is supported by DOE-AFCI (DE-FC07-08ID14926) and DOE-BES (DE-FG02-06ER15777). We would like to thank the reviewers for their critical suggestions regarding the interpretation of the data as well as the possible correlation between the properties of the core−shell structured particles and the observed structural and electronic structures.

Supporting Information Available: Comparison of the EELS spectra collected on the core−shell Fe particles in the present work with that of known iron oxide and literature data. Collective data show the TEM and STEM-HAADF images of the core−shell particles and the corresponding EELS spectrum from each particle collected using both JEOL JEM 2010 TEM and FEI aberration-corrected Titan 80−300 kV TEM/STEM. This material is available free of charge via the Internet at http://pubs.acs.org.

JA900353F

(71) Li, L.; Fan, M. H.; Brown, R. C.; Van Leeuwen, J. H.; Wang, J. J.; Wang, W. H.; Song, Y. H.; Zhang, P. Y. *Crit. Rev. Environ. Sci. Technol.* **2006**, *36*, 405–431.
(72) Kadossov, E.; Funk, S.; Burghaus, U. *Catal. Lett.* **2008**, *120*, 179–183.
(73) Baker, C.; Shah, S. I.; Hasanain, S. K. *J. Magn. Magn. Mater.* **2004**, *280*, 412–418.
(74) Spaldin, N. A. *Magnetic Materials*, 1st ed.; Cambridge Unversity Press: New York, 2003.